Report No. NADC-90073-60

FLEXURAL FATIGUE BEHAVIOR OF ARALL® LAMINATES

Jeffrey Cook and Mary Donnellan
Air Vehicle and Crew Systems Technology Department (Code 6063)
NAVAL AIR DEVELOPMENT CENTER
Warminster, PA 18974-5000

1 AUGUST 1990

FINAL REPORT
Period Covering 1 June 1989 to 1 August 1990
Task No. R34500000
Work Unit No. ZP100
Program Element No. 62234N
Project No. NA2A

Approved for Public Release; Distribution is Unlimited

Prepared for
Airborne Materials Block (Code 60C)
NAVAL AIR DEVELOPMENT CENTER
Warminster, PA 18974-5000

NOTICES

REPORT NUMBERING SYSTEM — The numbering of technical project reports issued by the Naval Air Development Center is arranged for specific identification purposes. Each number consists of the Center acronym, the calendar year in which the number was assigned, the sequence number of the report within the specific calendar year, and the official 2-digit correspondence code of the Command Officer or the Functional Department responsible for the report. For example: Report No. NADC-88020-60 indicates the twentieth Center report for the year 1988 and prepared by the Air Vehicle and Crew Systems Technology Deartment. The numerical codes are as follows:

CODE	OFFICE OR DEPARTMENT
00	Commander, Naval Air Development Center
01	Technical Director, Naval Air Development Center
05	Computer Department
10	AntiSubmarine Warfare Systems Department
20	Tactical Air Systems Department
30	Warfare Systems Analysis Department
40	Communication Navigation Technology Department
50	Mission Avionics Technology Department
60	Air Vehicle & Crew Systems Technology Department
70	Systems & Software Technology Department
80	Engineering Support Group
90	Test & Evaluation Group

PRODUCT ENDORSEMENT — The discussion or instructions concerning commercial products herein do not constitute an endorsement by the Government nor do they convey or imply the license or right to use such products.

Reviewed By: Jeffrey Waldman **Date:** 12/19/90
Branch Head

Reviewed By: [signature] **Date:** 2/5/91
Division Head

Approved By: [signature] **Date:** 2/11/91
Director/Deputy Director

Unclassified
SECURITY CLASSIFICATION OF THIS PAGE

REPORT DOCUMENTATION PAGE

Form Approved
OMB No 0704-0188

1a REPORT SECURITY CLASSIFICATION Unclassified	1b RESTRICTIVE MARKINGS
2a SECURITY CLASSIFICATION AUTHORITY	3 DISTRIBUTION / AVAILABILITY OF REPORT Approved for Public Release; Distribution is Unlimited
2b DECLASSIFICATION / DOWNGRADING SCHEDULE	
4 PERFORMING ORGANIZATION REPORT NUMBER(S) NADC-90073-60	5 MONITORING ORGANIZATION REPORT NUMBER(S)
6a NAME OF PERFORMING ORGANIZATION Air Vehicle and Crew Systems Technology Department 6b OFFICE SYMBOL (If applicable) 6063	7a NAME OF MONITORING ORGANIZATION
6c ADDRESS (City, State, and ZIP Code) NAVAL AIR DEVELOPMENT CENTER Warminster, PA 18974-5000	7b ADDRESS (City, State and ZIP Code)
8a NAME OF FUNDING / SPONSORING ORGANIZATION Airborne Materials Block 8b OFFICE SYMBOL (If applicable) 60C	9 PROCUREMENT INSTRUMENT IDENTIFICATION NUMBER
8c ADDRESS (City, State, and ZIP Code) NAVAL AIR DEVELOPMENT CENTER Warminster, PA 18974-5000	10 SOURCE OF FUNDING NUMBERS PROGRAM ELEMENT NO: 62234N PROJECT NO: NA2A TASK NO: R34500000 WORK UNIT ACCESSION NO: ZP100

11 TITLE (Include Security Classification)
Flexural Fatigue Behavior of ARALL-4® Laminates

12 PERSONAL AUTHOR(S)
Jeffrey Cook and Mary E. Donnellan

13a TYPE OF REPORT	13b TIME COVERED	14 DATE OF REPORT (Year, Month, Day)	15 PAGE COUNT
Final	FROM 6/1/89 TO 8/1/90	1990, August 1	

16 SUPPLEMENTARY NOTATION

17 COSATI CODES			18 SUBJECT TERMS (Continue on reverse if necessary and identify by block number)	
FIELD	GROUP	SUB-GROUP	ARALL	LAMINATE
			Flexural Fatigue	Delamination
			Salt Fog Exposure	Fiber Failure

19 ABSTRACT (Continue on reverse if necessary and identify by block number)

Axial fatigue testing has shown that ARALL® laminates possess outstanding fatigue resistance compared to monolithic aluminum alloys in tension-dominated cycling. This work examines the fatigue behavior of 3/2 and 5/4 ply ARRALL-4® in pure flexure (R=-1). The effect of salt-fog exposure on fatigue response was also investigated. Results indicate that, in general, failure occurs in three stages: cracking of the outer aluminum surfaces, delamination at the interfaces between fiber-rich and resin-rich regions, and fiber failure. The flexural fatigue resistance of ARALL-4® was found to be excellent; compressive stresses did not contribute significantly to failure of the laminates.

20 DISTRIBUTION AVAILABILITY OF ABSTRACT	21 ABSTRACT SECURITY CLASSIFICATION
☒ UNCLASSIFIED UNLIMITED ☐ SAME AS RPT ☐ DTIC USERS	Unclassified
22a NAME OF RESPONSIBLE INDIVIDUAL Jeffrey Cook	22b TELEPHONE (Include Area Code) (215) 441-1509 22c OFFICE SYMBOL 6063

DD Form 1473, JUN 86 *Previous editions are obsolete*

S/N 0102-LF-014-6603

SECURITY CLASSIFICATION OF THIS PAGE
Unclassified

CONTENTS

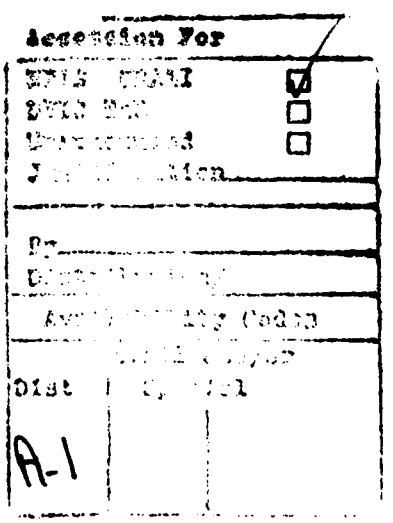

FIGURES

TABLES

ACKNOWLEDGEMENTS

The authors wish to thank G. Connelly and Lehigh University for the facilities and assistance in optical imaging; and W. Worden for his artistic contribution.

INTRODUCTION

Numerous studies have been conducted to characterize the fatigue properties of ARALL laminates. These studies have concentrated primarily on tension-tension axial fatigue. Under these conditions, ARALL possesses outstanding fatigue properties as compared to monolithic aluminum alloys[1,2]. The excellent fatigue resistance is primarily due to bridging of the fatigue crack by aramid fibers in the prepreg layer[2,3]. Crack bridging blunts the stress concentration at the crack tip, greatly reducing the crack growth rate. This mechanism is effective in both axial and flexural fatigue, because in both cases the direction of crack propagation is perpendicular to the fiber alignment.

Some degree of delamination at the interface between the fiber-rich and resin-rich layers in the vicinity of the crack has been found to be desirable. Delamination prevents premature failure of the aramid fibers by reducing the crack bridging stresses in the fibers near the crack tip, and distributing the stresses more evenly through the fiber prepreg layer[2].

Fatigue studies incorporating compressive stresses have generally not been applied to ARALL, because of the poor properties of Aramid fibers in compression[4]. Aramid fibers are extremely susceptible to microbuckling when compressed; this destroys the excellent fatigue and strength properties they possess in tension. This problem is compounded in some ARALL variants by the unfavorable stress state incurred during the curing process. Curing is performed at an elevated temperature, and when the laminate is cooled to room temperature, a residual tensile stress exists in the aluminum layers, with a corresponding compressive stress in the prepreg layers[2].

Some ARALL laminates are subjected to a 0.4 percent stretch after curing, to eliminate this unfavorable stress state. Stretched ARALL has a residual compressive stress in the aluminum layers, and a residual tensile stress in the aramid fibers. When the laminate is subjected to compression, these residual stresses reduce the compression experienced by the fibers, and increase that experienced by the aluminum layers. This results in improved compressive fatigue properties as compared to ARALL which was not stretched. Flexural fatigue tests (R = -1) performed by Hasson[5] on prestretched ARALL-1^{R} (using 7075 aluminum, rather than 2024) have demonstrated superior fatigue resistance to monolithic 7075 at all stress levels up to nearly 350 MPa (50 ksi).

Moisture absorption tests performed on ARALL laminates have shown[6,7] that the outermost aluminum layers act as barriers to moisture absorption. As a result, moisture absorption is very low as compared to other composite materials. There is, therfore, only a slight reduction in tensile strength upon exposure to moist and corrosive environments[7,8].

The flexural fatigue tests performed in the current work were aimed, in part, at investigating the compressive fatigue properties of ARALL-4®, which was not stretched after curing. In addition, the sequence and relative importance of various failure mechanisms were investigated under various environmental conditions. All tests were performed at a nominal stress of 221 MPa (32 ksi), which is equal to one half the yield stress of ARALL-4® at ambient temperature[8]. The results of this work serve as a general assessment of the suitability of ARALL-4® in applications involving flexural stresses and exposure to a corrosive environment.

EXPERIMENTAL PROCEDURE

High cycle flexural fatigue tests were performed using Tatnall-Krouse flexural fatigue machines, which are capable of a maximum load of 40 lbs and an operating speed of 30 cycles per second. The specimen configuration and dimensions are shown in Figure 1. Specimens were cut from a unidirectional ARALL-4® sheet, and an aluminum sheet. The test equipment is shown in Figure 2.

Three different material configurations were examined: (1) 3/2 ply ARALL-4® (3 layers of aluminum alternating with 2 layers of aramid/epoxy prepreg), (2) 5/4 ply ARALL-4®, and (3) a 2024-T81 sheet. Thicknesses were 1.32mm (.052 in), 2.34mm (.092 in), and 1.02mm (.040 in) respectively. ARALL-4® is comprised of anodized and primed 2024-T8, and aramid fiber reinforced epoxy prepreg layers.

All three materials were tested in the longitudinal (0 degree) and transverse (90 degree) directions. These directions refer to the fiber orientation in the unidirectional ARALL laminates, and to the rolling direction in the aluminum sheet. Specimens are identified by a four digit number. The first two digits represent the number of aluminum and aramid laminae, the third identifies the orientation as longitudinal or transverse, and the fourth is the sequential number of the specimen in a series of eight identical specimens. Thus, the 3/2 ARALL specimens cut in the 0 degree direction are numbered 3201 through 3208. Similarly, the 5/4 specimens cut in the 90 degree direction, are 5491 through 5498. The whole series of eight specimens is designated 5490 type. The aluminum sheet specimens, for consistancy, are designated the 1000 and 1090 types.

All three materials in the 0 degree and 90 degree orientations were tested in the as-cut condition from the sheet. Similar tests were performed after exposing the specimens to a salt-fog environment for two days (one day on each side). The specimens were tilted at 7 degrees from vertical during exposure. Excess salt was removed from the specimens following exposure, by gently abrading the surface. The preferred nitric acid bath technique was not used due to possible damage to, or absorption by, the aramid layers in the ARALL specimens.

Half of the salt-fog exposed specimens were exposed with bare edges, while the other half were exposed with their edges sealed to prevent moisture absorbtion by the aramid layers. An RTV (Room-Temperature Vulcanizing) silicone-based sealant was used for sealing the specimens. Table 1 shows the specimens tested in each of the three conditions.

Tests on all specimens were begun at an initial maximum stress of ±221 MPa (32 ksi), with both sides of the specimen subjected to equal tensile and compressive loads (R=-1). This surface stress level, S, was used as a reference point for data collected subsequently. The initial stress is calculated based on the specimen dimensions, the load on the specimen, and a correction factor F, which corrects for the variation in modulus from one layer to the next in the ARALL specimens:

$$S = \frac{6LW}{bd^2F}$$

where, S is stress at the surface, L and b are dimensions specific to the type of specimen, d is specimen thickness, and W is the initial load on the specimen. A sample of the calculations used to determine F for each type of specimen is shown in Appendix A. The deflection of the specimen caused by the load W, was measured using a dial gauge micrometer accurate to 0.01 mm. The fatigue machine was set for this deflection.

Since the specimens were fatigued at constant deflection, the load on the specimen decreased as fatigue damage accumulated. The load on the specimen was measured periodically by hanging weights

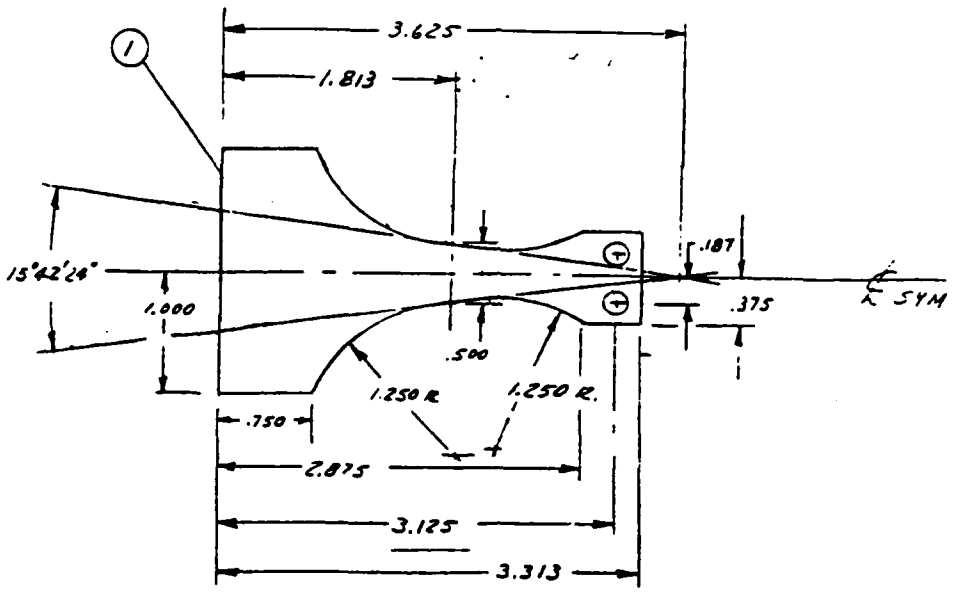

Figure 1. Specimen Configuration for Flexural Fatigue Testing.

Table 1.

Specimens and Conditions for Fatigue Testing.

Condition	2024 Sheet	3/2 ARALL	5/4 ARALL
Unexposed	1001,1002, 1091,1092	3202,3203, 3292,3293	5401,5402, 5491,5492
Exposed, Bare Edges	1003,1004, 1093,1094	3204,3205, 3294,3295	5403,5404, 5493,5494
Exposed, Sealed	--------- ---------	3206,3207, 3296,3297	5405,5406, 5495,5496

on the specimen as shown in Figure 2. Cycling was continued until ten million cycles was reached or until the specimen failed (i.e., breakage or inability to support any load).

Low-magnification photographs were taken of representative specimens upon completion of testing. A Polaroid MP-3 land camera was used. Photographs recorded surface conditions and surface crack morphologies of the specimens.

Some of the fatigued specimens were inspected optically by using a Questar telescope, linked via a CCD camera to a real-time computer display. The exposed edges of the layers in each specimen were observed in the loaded and unloaded conditions to characterize cracking and delamination phenomena. The effects of the different fatigue testing conditions (i.e.,unexposed,etc.) on these phenomena were determined.

Scanning Electron Microscopy (SEM) was used to examine interfacial cracking, delamination, and fiber deformation or failure. An AMRAY 1000B microscope with an accelerating voltage of 20kV was used.

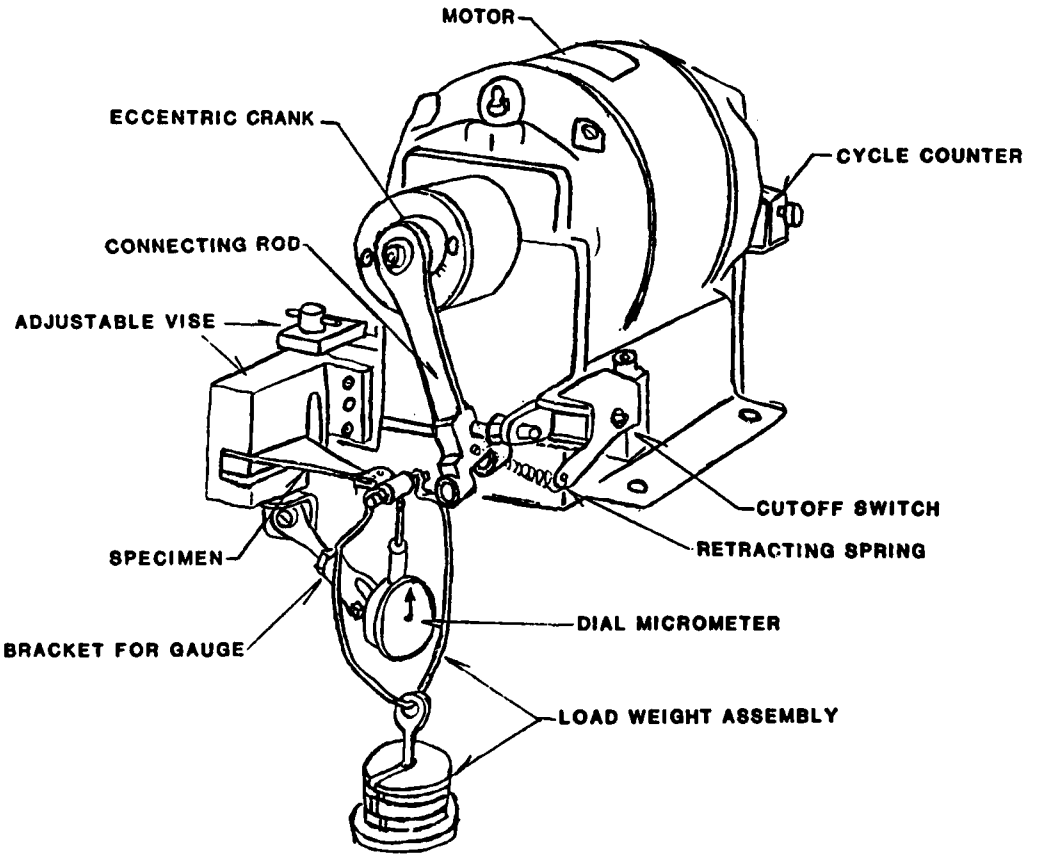

Figure 2. Tatnall-Krouse Flexural Fatigue Machine with Load Weights and Dial Micrometer Attached for Deflection Measurement. For Fatigue Cycling, these are removed, and the Connecting Rod is Reconnected to the Specimen.

EXPERIMENTAL RESULTS

FLEXURAL FATIGUE

Unexposed Condition: Plots showing surface stress as a function of the number of fatigue cycles for the unexposed longitudinal specimens are shown in Figure 3a. The 2024 sheet specimens, 1001 and 1002, failed entirely after 2.5×10^5 cycles; failure occurred almost immediately after surface cracks appeared in the specimens. Specimens 3202 and 3203 (3201 was invalid due to an error in load measurement) showed a slight reduction in stress up to about 5×10^5 cycles. At that point, both experienced a rapid drop in load which became less severe after about 2×10^6 cycles. The drop-off in load corresponded to the appearance of one or two deep transverse cracks on the top and bottom surfaces of the specimens, and a visible delamination at the uppermost resin/aluminum interface.

Specimens 5401 and 5402 differed from the 3200-type specimens in that they showed not one, but two distinct drops in load. The first drop from the initial 221 MPa (32 ksi) occurred at 80,000 cycles in 5402, and leveled off at 180 MPa (26 ksi). This first drop coincided with the formation of about a half dozen fine cracks in the outer aluminum layer. These cracks were spaced more closely than in the two 3200-type specimens. Both 5400-type specimens experienced a sharp second drop after a half million cycles, and leveled out at 80 MPa (12 ksi). None of the four unexposed longitudinal ARALL specimens broke completely through, but were held together by the aramid/epoxy layers, and in some cases, by the middle aluminum layer, as well.

The transverse unexposed specimens, as shown in Figure 3b, all failed between 1.5 and 2.5×10^5 cycles. The 3/2 ARALL specimens, like the 2024 sheet, reached a certain number of cycles and then failed immediately after cracks appeared in the outer surface. The 5/4 specimens cracked very deeply, but remained intact to above 120 MPa (17 ksi) for a short time before failure. All transverse specimens failed completely (i.e., all layers fractured such that the specimen could support no load).

Salt-Fog Exposed--Bare Edges: Figure 4a shows plots of stress versus number of cycles for longitudinal specimens which were exposed to salt-fog for two days prior to testing. The 2024 sheet specimens behaved similarly to those in the unexposed condition, except that surface cracks began forming almost immediately. One of the cracks continued to deepen until specimen failure occurred at about 80,000 cycles.

Specimens 3204 and 3205 both showed a rapid drop in load after 20,000 cycles, which leveled out near 110 MPa (16 ksi), or 50 percent of the original stress, after 10^6 cycles. This level was maintained through 10^7 cycles.

Specimens 5403 and 5404 showed a continuous drop in load as the test proceeded. Unlike the 3/2 specimens above, the load on the 5/4 specimens continued decreasing through 10^7 cycles. Specimen 5403 failed entirely; this was the only longitudinal ARALL specimen tested in which this occurred.

The transverse 2024 specimens, 1093 and 1094, failed in nearly identical fashion to their longitudinal counterparts at 80,000 cycles (Figure 4b). The loads on the 3/2 and the 5/4 ARALL specimens dropped continuously until failing between 50,000 and 80,000 cycles at 130 MPa (19 ksi). The stress experienced by the 3/2 specimens decreased more rapidly than that in the 5/4 specimens.

Salt-Fog Exposed--Sealed Edges: The longitudinal 3/2 specimens exposed with sealed edges, behaved identically to those exposed with bare edges (Figure 5a). Specimens 5405 and 5406 experienced the same initial drop-off as their bare-edged counterparts, but then leveled off at 150 MPa (22ksi) after 2×10^5 cycles. Both specimens experienced a sudden drop to 90 MPa at 6.5×10^6 cycles.

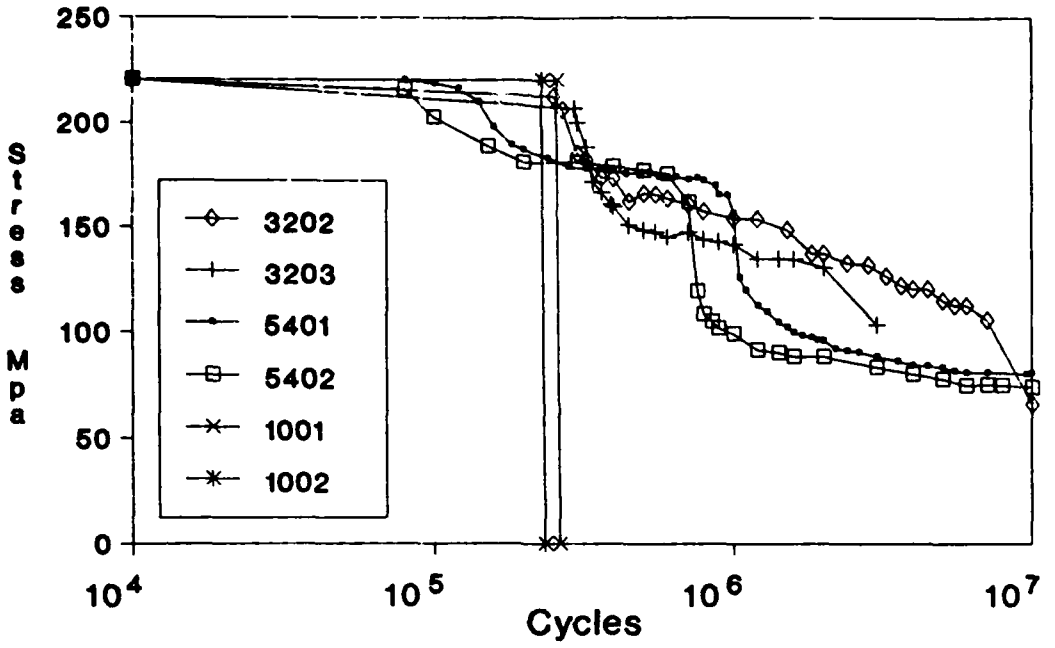

Figure 3a. Load Versus Number of Cycles for Unexposed Longitudinal Specimens.

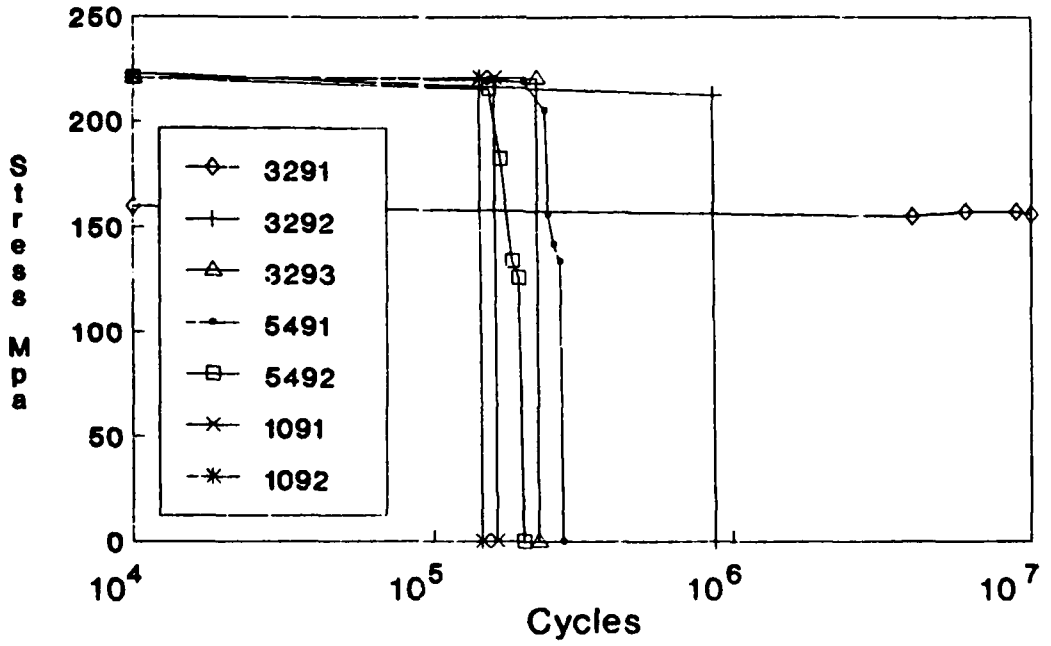

Figure 3b. Load Versus Number of Cycles for Unexposed Transverse Specimens.

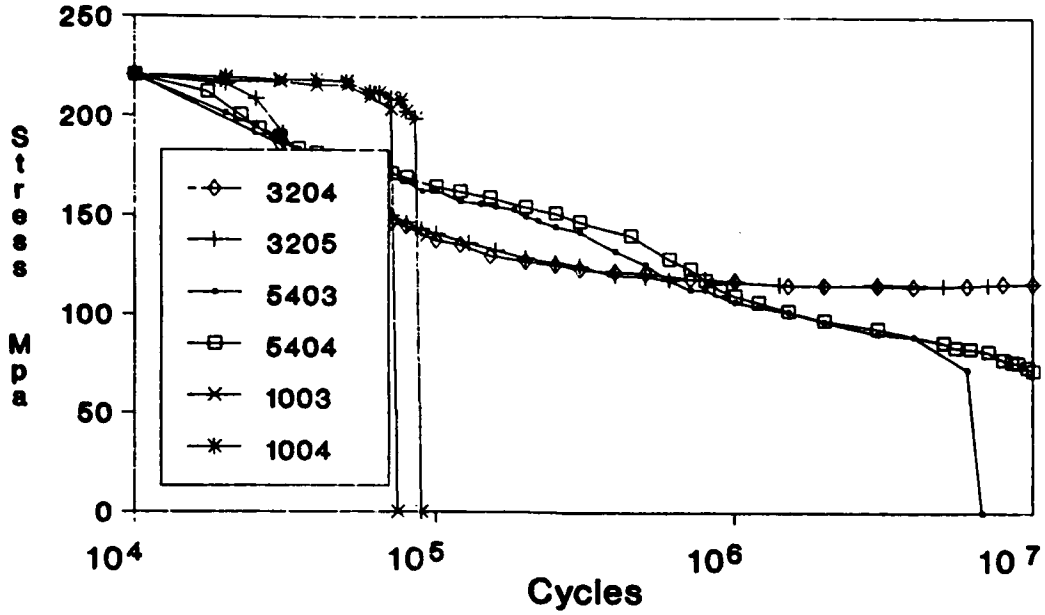

Figure 4a. Load Versus Number of Cycles for Longitudinal Specimens Exposed with Bare Edges.

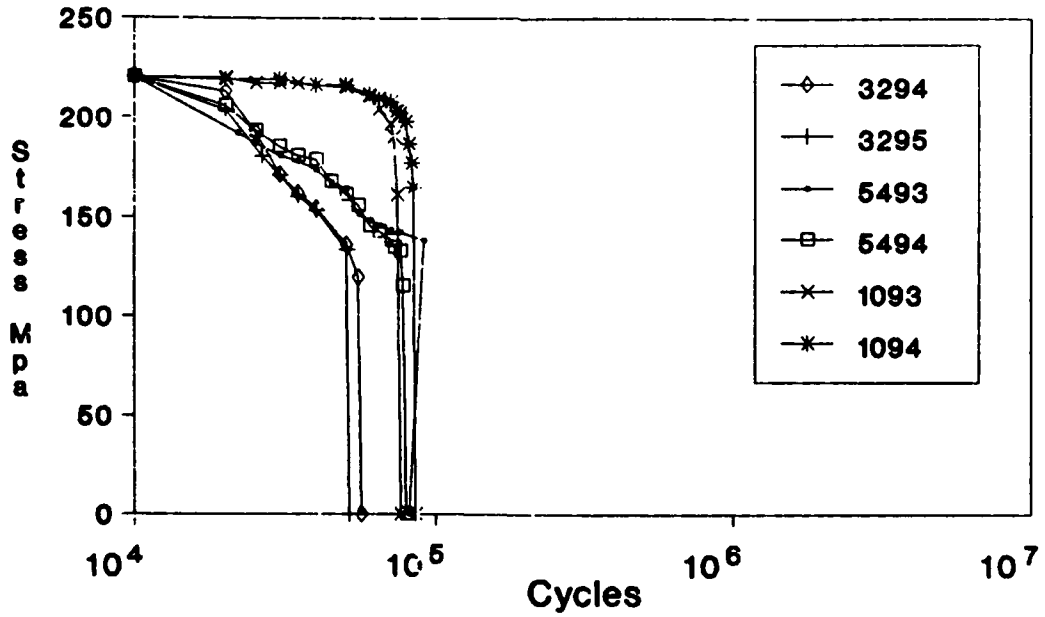

Figure 4b. Load Versus Number of Cycles for Transverse Specimens Exposed with Bare Edges.

The transverse specimens, Figure 5b, behaved similarly to those exposed with bare edges.

MICROSCOPY

Macrophotography: Low-magnification photographs of the fatigued specimens showed a wide range of surface crack morphologies. Specimen 3203 (unexposed) showed two well-defined cracks, separated by about 6mm, on each side (Figure 6). Specimen 3202 was similar. Specimens 5401 and 5402 were tested in the same condition, but showed nearly a half dozen cracks on each side. These cracks were spaced 3 to 4mm apart. Transverse (unexposed) specimens typically had a single surface crack, and fractured all the way through at or near this crack (Figure 7).

The salt-fog exposed specimens, with both sealed and unsealed edges, showed very different surface cracking from the unexposed ones. Longitudinal 3/2 specimens had no visible cracks on either side at low magnification. The 5/4 specimens contained a series of very fine cracks; these were difficult to resolve in the photographs, but at least 16 were visible in specimen 5404 (Figure 8). These cracks were 1 to 2mm apart. Transverse specimens in the exposed conditions, revealed a single crack at the fracture point, as did their unexposed counterparts. The cracks in the exposed specimens were jagged and discontinuous, apparently following the grain boundaries in the aluminum.

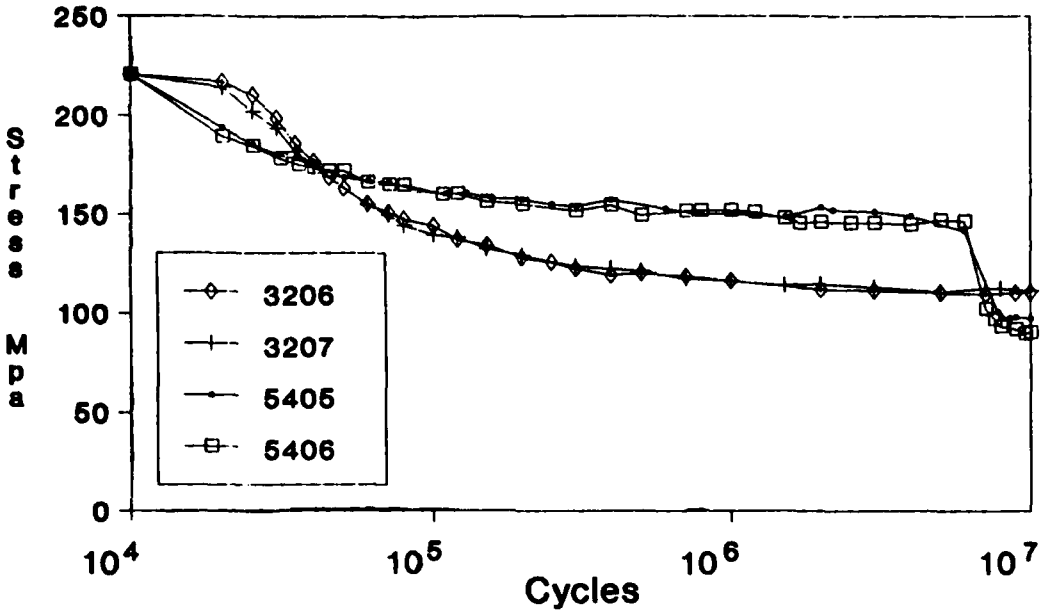

Figure 5a. Load Versus Number of Cycles for Longitudinal Specimens Exposed with Sealed Edges.

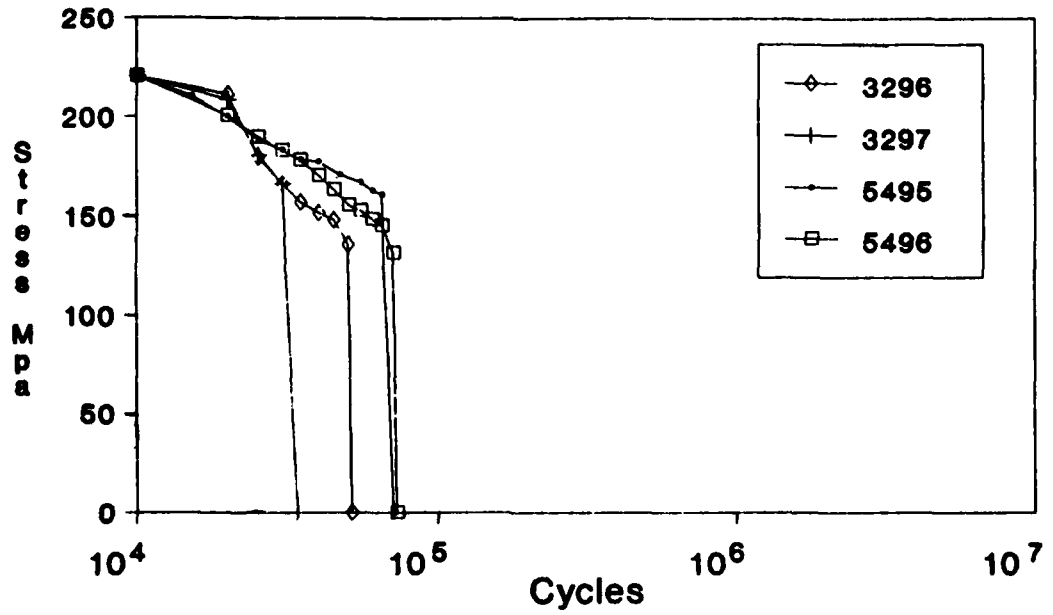

Figure 5b. Load Versus Number of Cycles for Transverse Specimens Exposed with Sealed Edges.

Figure 6. Surface Cracks in Specimen 3202 (10^7 cycles).

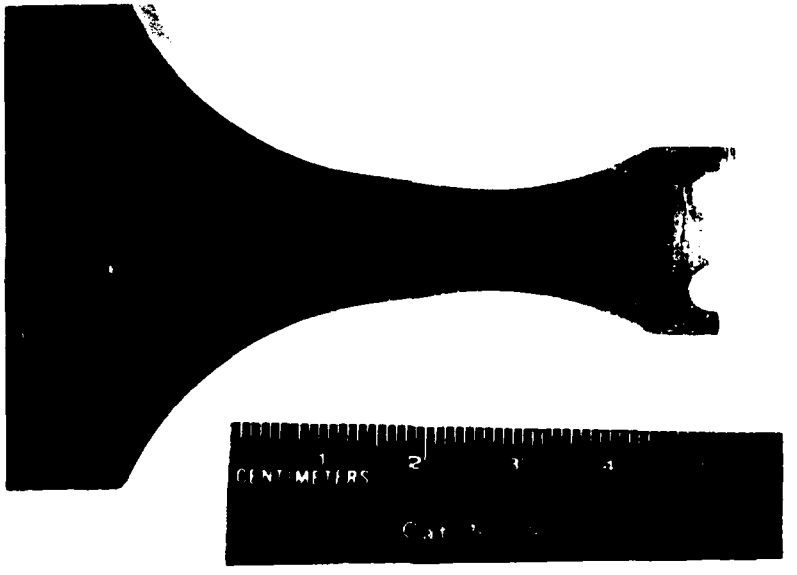

Figure 7. Fracture of Specimen 3292 (8.6 X 10^5 cycles).

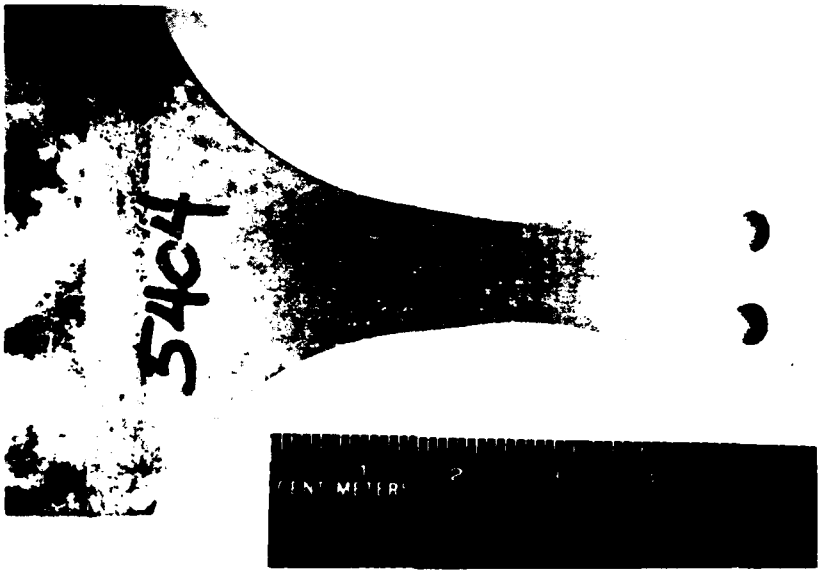

Figure 8. Surface Corrosion and Fine Surface Cracking in Specimen 5404 (10^7 cycles).

Optical Imaging: Observations of the different ARALL layers (exposed on the edges of the specimens) in different fatigued specimens, revealed varying degrees of delamination from one specimen to the next. The unexposed specimens, revealed cracks through both the aluminum and prepreg layers, as well as delamination along the interfaces. The cracks running through the fiber layers were diagonal, and did not occur directly under the cracks in the overlying aluminum layers. By applying a bending load to the specimen, cracks were observed to open up in the aluminum, and at fiber failure locations in the prepreg. Wherever delamination was observed, the laminae could be seen sliding relative to each other, when a load was applied.

The exposed 3/2 specimens revealed many fine cracks in the outermost aluminum layer, but no delamination, sliding, or fiber failure was observed, regardless of whether edges were sealed or bare. Specimen 5404 (bare edges) showed no fiber failure, but all of the aluminum layers were cracked, and extensive sliding was observed between the aluminum and prepreg layers, when a load was applied. Specimen 5405 (sealed edges), on the other hand, showed little delamination, but the outer fiber layers had failed.

Scanning Electron Microscopy: Figure 9 shows the outermost aramid layer from specimen 3202. A half-inch section of the outer aluminum layer was cut from the specimen and lifted off; the surface shown, is that created along fatigue delaminations. Failure occurred at the interface between the fiber-rich and resin-rich epoxy layers.

Figure 10 shows the primary fatigue crack on the outermost aramid surface in 3202. The crack through the overlying aluminum layer, was almost directly on top of that through the aramid layer. This

image demonstrates the bridging of the crack by the aramid fibers. Although these fibers were subjected to both tensile and compressive loads during cycling, there is no sign of fiber buckling or other damage after $2x10^6$ cycles.

Figure 9. SEM Micrograph of Aramid Fibers in 3202.

Figure 10. Crack-bridging by Aramid Fibers in 3202.

The outermost aluminum/aramid interface of specimen 5403 is shown in Figure 11. This was the only longitudinal specimen which failed completely; Figure 11 shows the fractured surfaces. The crack running through the image is due to delamination during fatigue. The delamination did not occur at the aluminum/epoxy interface, but rather at the interface between the aramid fibers and the resin-rich adhesive layer. This was found to be the case in all other specimens which contained significant delaminations. It is along this boundary that the interlaminar sliding seen during optical imaging occurred.

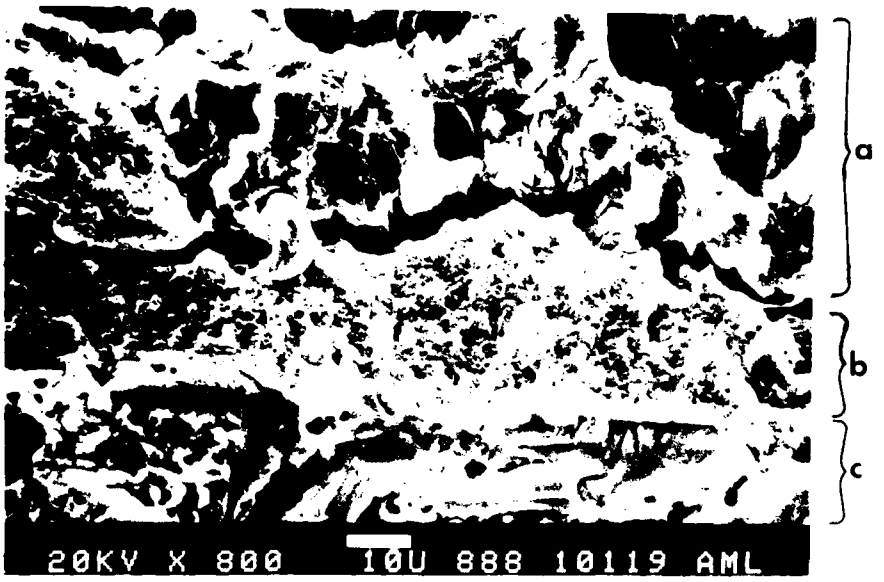

Figure 11. Fracture Surface of 5403, Showing from Top to Bottom:
a) Aramid/epoxy Prepreg Layer; b) Resin-rich Epoxy Layer;
c) 2024-T8 Aluminum Layer.

DISCUSSION OF RESULTS

2024 SHEET:

The 2024 aluminum sheet behaved as expected. Exposure to the salt-fog environment resulted in a two-thirds reduction in the fatigue life of the longitudinal specimens. The reduction was about one half for the transverse specimens. These reductions were the result of corrosion of the outer surface of the aluminum, which greatly increased the number of crack initiation sites through the formation of surface pits. Cracks form much more readily in the corroded specimens than in the relatively smooth unexposed ones. Typical of monolithic aluminum, specimen failure proceeded rapidly following the formation of surface cracks.

TRANSVERSE ARALL:

Fatigue failure of the transverse specimens was similar to the 2024 sheet. In the transverse direction, neither the fibers nor the epoxy adhesive contributed to the fatigue strength of the ARALL. The epoxy, since it carries relatively little load in tension, serves only to blunt transverse cracks. This explains the shape of the ARALL curves in Figures 4b and 5b, which indicate that the aluminum layers fail sequentially from outermost to innermost. In the transverse direction, ARALL-4® was found to be more sensitive to moisture and salt-fog damage than the monolithic aluminum.

LONGITUDINAL ARALL:

3/2 ARALL, Unexposed: The initial drop in load in the unexposed specimens (Figure 3a) is the result of the formation of transverse cracks in the outermost aluminum layers. Crack formation reduces the stiffness and the effective load-carrying thickness of the specimen. The subsequent steady drop in load, is attributed to steady delamination at the outer fiber/epoxy interfaces, and in later stages, to fiber breakage in the prepreg layer as well.

The extensive delaminations observed in these specimens (as much as three quarters of an inch on each side of the main crack) are a result of buckling of the outer aluminum layer in the compression segment of the fatigue cycle. It has been observed that in tension, delamination is attributable primarily to Mode I fatigue stresses[9]. In the compression segment of the fatigue cycle, buckling of the aluminum layer bends it away from the underlying prepreg layer, increasing the Mode I stresses on the interface. The buckling in the 3/2 specimens was pronounced, because a relatively large deflection (roughly 0.35 inch on the specimen in Figure 1) was required to achieve an initial load of 32 ksi (221 MPa).

3/2 ARALL, Exposed: After exposure to salt spray, cracks formed in the outer aluminum layers much sooner than in the unexposed specimens. In unexposed specimens, having only one or two cracks, the majority of the deflection imposed on the specimen was accommodated by a sharp bend at the location of the cracks. This increased both the Mode I stresses at the interfaces, and the severity of the local bending stresses on the fibers. In the exposed specimens, the multiple, fine surface cracks reduced Mode I and II stresses and distributed the bending more evenly along the interfaces and the fibers, thus no significant delamination or fiber breakage occurred. This in part explains why the exposed specimens maintained a higher load than the unexposed specimens beyond 2.5×10^6 cycles.

There was no difference in behavior between specimens exposed with bare and sealed edges. With the formation of the many stress-relieving cracks in the aluminum, the stress at the interfaces was insufficient tc cause delamination despite any weakening effect from moisture absorption.

5/4 ARALL, Unexposed: As in the 3/2 material, the initial drop in load is due to cracking of the surface layers. The second, more severe drop in the unexposed specimens can be attributed to

delamination and fiber failure in the outermost prepreg layers. The nominal stress in these layers is much higher than in the 3/2 prepreg layers, because they are closer to the surface relative to the thickness of the material than in the 3/2 (see Appendix A). The steep load drop indicates that failure of the fiber layers occurred over a small number of cycles as compared to the 3/2 material. Delamination at all fiber-rich/resin-rich interfaces occurred simultaneously with fiber failure. The extent of delamination due to buckling of the outer aluminum layers was not as severe as in the 3/2, because a smaller deflection was required for the initial loading.

While the compressive stress (as well as the tensile stress) in the outermost prepreg layers was higher than in the 3/2 specimens, SEM imaging of fibers exposed by delamination showed no sign of buckling or other compression damage in the fibers. The compressive loads are taken up mainly by the aluminum, the cracked surfaces impinging upon each other when compressed. During tension, however, the cracks open up, leaving the fibers to support the tensile load. This causes the neutral (stress-free) axis of the specimen to always move closer to the surface in compression. The result, is that once surface cracking has occurred, the normal stresses in the fiber layers are predominantly tension, rather than compression. Calculations of the maximum stresses encountered following failure of the aluminum layers are shown in Appendix B.

Failure of the prepreg layers in the unexposed 5/4 specimens occurred in close proximity to the major cracks in the overlying aluminum layers, and to corresponding crack-bridging locations in the prepreg layer as well. These observations indicate that fiber failure in these specimens was due to increased tensile load on the fibers in the vicinity of cracks, and that compressive stresses did not contribute significantly to fiber failure.

In axial fatigue tests incorporating compressive loads, compressive fiber damage would be expected at a much lower stress level than in flexure (R=-1), due to the reduction of compressive loads in flexure as described above. Studies have shown[1] that ARALL-1® with a 0.5 percent prestretch, posesses outstanding fatigue properties compared to 7050-T76 in both FALSTAFF and Mini-TWIST fatigue spectra. Maximum compressive loads in these spectra were as high as 69 MPa (10 ksi) (R=-0.25).

5/4 ARALL, Exposed: Salt-fog exposure caused surface cracking in 5/4 ARALL to occur much more quickly, just as in the 3/2 material and the 2024 sheet. However, moisture absorbtion at lamellar interfaces was found to have a major influence on fatigue resistance in the thicker material. Specimens exposed with bare edges, showed a continuous drop in load as extensive delamination occurred at all fiber-rich/resin-rich interfaces. The interfaces were weakened so much by moisture absorbtion that they could not withstand the loads encountered during cycling. The delamination greatly decreased the degree of constraint on the lamina, with the resulting loss in load-carrying ability. The interfaces in the specimens exposed with sealed edges were not weakened, and the fatigue load maintained by these specimens, like the exposed 3/2 specimens, leveled off after only a small amount of delamination had occurred. After 6 to 7 million cycles, the outermost aramid layers failed. Since very little delamination occurred, and the load on the specimen remained higher, the fibers were supporting a much higher load during cycling than in specimens with bare edges.

EFFECT OF SALT-FOG EXPOSURE:

It can be seen from these experiments that at the intermediate stress levels investigated, exposure to salt spray can actually improve the fatigue properties of ARALL by causing multiple surface crack formation. Multiple surface cracking relieves the stresses responsible for large scale delamination, and also distributes bending strains more evenly along the specimen. The result is that delamination and failure of the aramid fibers are delayed or prevented, and thus no catastrophic failure of the laminate occurs.

On the other hand, it was found that above a certain stress level, moisture absorbtion at the laminar interfaces can weaken the fiber-rich/ resin-rich interfaces enough to cause severe delamination. This destroys the load carrying ability of the material without any readily visible signs of fatigue damage. The severe delaminations and fiber failure encountered in some of the specimens tested would become more prevalent at higher initial stresses. At lower stresses, Hasson[5] reports a runout stress of about 186 MPa (27 ksi) for prestretched ARALL-1 in the longitudinal direction (about 110 MPa/16 ksi in the transverse direction). One transverse specimen tested in this study (3291) showed no sign of load drop or cracking after 10^7 cycles at 160 MPa (23.2 ksi).

At flexural stresses up to roughly half the yield stress of the material (YS = 440 MPa/64 ksi in the longitudinal direction), surface cracking occurs as in any monolithic aluminum sheet, but the crack-bridging aramid fibers provide virtually unlimited resistance to through-thickness failure of the laminate. In this sense, ARALL offers a distinct advantage over conventional aluminum alloy sheet.

STRESSES ENCOUNTERED DURING FATIGUE:

Appendix B shows that, after the outermost aluminum layers have failed, the prepreg layers in 3/2 ARALL experienced maximum tensile and compressive stresses of 219 MPa (31.7 ksi) and 83 MPa (12 ksi) respectively (R=-0.38). This is a substantial deviation from the ±106 MPa (15.4 ksi) before surface cracking (Appendix A). In the 5/4 ARALL, the maximum post-cracking stresses on the outermost prepreg layers were 272 MPa (39.5 ksi) tensile, and 139 MPa (20.1 ksi) compressive (R=-0.51), compared to ±146 MPa (21.2 ksi) before cracking.

It is important to note that these results were obtained using unstretched ARALL-4®, where there is a pre-existing compressive stress in the prepreg layers. The calculations above use loads estimated from the experimental load data, and do not take into account the increased compliance due to delamination or non-longitudinal deformation of the prepreg layers in compression. Nonetheless, the results demonstrate the ability of ARALL to withstand relatively large compressive loads in fatigue without incurring compressive fiber damage. The higher prepreg loads experienced by the 5/4 ARALL both before and after surface cracking, also explain the better fatigue response of the 3/2 configuration.

CONCLUSIONS

1. In the longitudinal (0°) direction, ARALL-4® posesses superior flexural fatigue properties as compared to monolithic 2024-T8 aluminum. Failure of the ARALL generally involves, in order of occurrence, cracking of the aluminum layers, delamination, and fiber breakage.

2. In the transverse (90°) direction, ARALL-4® and 2024-T8 aluminum possess similar fatigue behavior.

3. Salt-fog exposure of ARALL leads to the formation of multiple surface cracks, which greatly reduce the amount of delamination and fiber breakage that occurs during flexural cycling.

4. Moisture absorbtion weakens the fiber/resin interfaces, leading to increased delamination at the fiber-rich/resin-rich interfaces if the specimen edges are not sealed.

5. At the stress levels investigated, 3/2 ply ARALL-4® is more resistant to fiber failure and degradation by moisture absorbtion than is 5/4 ARALL-4®, due to the lower stresses at the interfaces and in the fibers.

6. ARALL-4® experiences no compressive fiber damage after 2×10^6 cycles at ±221 MPa (32 ksi), despite the presence of residual compressive stresses in the prepreg layers.

REFERENCES

1. Ruschau, John, "Fatigue Crack Growth Characteristics of ARALL-1^{R}," University of Dayton Research Institute, UDR-TR-88-21, May 1988.

2. Marissen, R., "Fatigue Crack Growth Predictions in Aramid Reinforced Aluminum Laminates (ARALL)," DFVLR, Institute for Materials Research, 1986.

3. Ritchie, R., Yu, W., and Bucci, R., "Fatigue Crack Propagation in ARALL Laminates: Measurement of the Effect of Crack-Tip Shielding from Crack Bridging," from Engineering Fracture Mechanics, Vol. 32, No. 3, 1989.

4. Langston, P., "Design and Use of Kevlar in Aircraft Structures," from SAE General Aviation Meeting and Exposition, Wichita, Ks, Apr. 1985.

5. Hasson, D., and Crowe, C., "Flexural Fatigue Behavior of Aramid Reinforced Aluminum 7075 Laminate (ARALL-1) and Al 7075 Alloy Sheet in Air and Salt Laden Humid Air," from Vol 2, ICCM & ECCM, London, July, 1987.

6. Verbruggen, M.L.C.E., "Moisture Absorption of ARALL," Delft University of Technology report LR-474, Aug. 1985.

7. Lee, S., and Kipp, T.R., "The Environmental Resistance of ARALL Laminates," from 20th International Sampe Technical Conference proceedings, Sept. 1988.

8. Donnellan, M.E., and Cook, J., "Evaluation of ARALL-4®, an Aramid Fiber Reinforced Aluminum Laminate," *Naval Air Development Center Report No. NADC-89100-60, Oct. 1989.*

9. Roebroeks, G., "Observation on Cyclic Delamination in ARALL under Fatigue Loading," Delft University of Technology, LR-496, Sept. 1986.

APPENDIX A

FLEXURAL STRESS ANALYSIS FOR UNFATIGUED ARALL

5400 TYPE- Before Cracking:

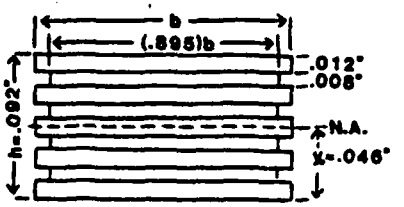

5400-type equivalent structure

$(\sigma_{max})_{al} = My/I$
$(\sigma_{max})_{pr} = nMy/I$

$n = E_{pr}/E_{al} = 9.5Msi/10.6Msi = 0.895$

$y_o = \Sigma Ay/\Sigma A = 0.046"$ (symmetry)

$I = \Sigma (bh^3/12 + Ad^2) = 3.160 \times 10^{-5}\ in^4$

* $(\sigma_{max})_{al} = My/I = (12.13\ lbs)(1.813")(\pm 0.046")/(3.160 \times 10^{-5})$
$= \underline{\pm 32.0\ ksi}$

* $(\sigma_{max})_{pr} = nMy/I = (0.895)(12.13)(1.813)(\pm 0.034)/(3.160 \times 10^{-5})$
$= \underline{\pm 21.2\ ksi}$

Correction Factor F for initial load calculation:

$F = I/I_o$ (I_o = bending moment of inertia for monolithic aluminum of same thickness and width)

$F = (3.160 \times 10^{-5}\ in^4)/(3.245 \times 10^{-5}\ in^4)$
* $\underline{F = 0.974}$

5490 TYPE- Before Cracking:

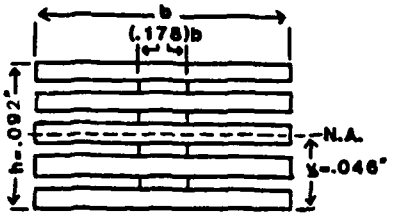

5490-type equivalent structure

$(\sigma_{max})_{al} = My/I$
$(\sigma_{max})_{pr} = nMy/I$

$n = E_{pr}/E_{al} = 1.9Msi/10.6Msi = 0.178$

$y_o = \Sigma Ay/\Sigma A = 0.046"$ (symmetry)

$I = \Sigma (bh^3/12 + Ad^2) = 2.580 \times 10^{-5}\ in^4$

* $(\sigma_{max})_{al} = My/I = (9.90\ lbs)(1.813")(\pm 0.046")/(2.580 \times 10^{-5})$
$= \underline{\pm 32.0\ ksi}$

* $(\sigma_{max})_{pr} = nMy/I = (0.178)(9.90)(1.813)(\pm 0.034)/(2.580 \times 10^{-5})$
$= \underline{\pm 4.2\ ksi}$

Correction Factor F for initial load calculation:

$F = I/I_o$
$F = (2.580 \times 10^{-5}\ in^4)/(3.245 \times 10^{-5}\ in^4)$
* $\underline{F = 0.795}$

3200 TYPE- Before Cracking:

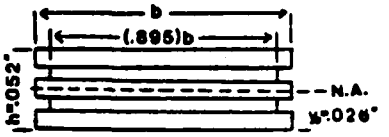

3200-type equivalent structure

$(\sigma_{max})_{al} = My/I$
$(\sigma_{max})_{pr} = nMy/I$

$n = E_{pr}/E_{al} = 9.5Msi/10.6Msi = 0.895$

$y_o = \Sigma Ay/\Sigma A = 0.026"$ (symmetry)

$I = \Sigma (bh^3/12 + Ad^2) = 5.770 \times 10^{-6}\ in^4$

* $(\sigma_{max})_{al} = My/I = (3.92\ lbs)(1.813")(\pm 0.026")/(5.770 \times 10^{-6})$
$= \underline{\pm 32.0\ ksi}$

* $(\sigma_{max})_{pr} = nMy/I = (0.895)(3.92)(1.813)(\pm 0.014)/(5.770 \times 10^{-6})$
$= \underline{\pm 15.4\ ksi}$

Correction Factor F for initial load calculation:

$F = I/I_o$
$F = (5.770 \times 10^{-6}\ in^4)/(5.859 \times 10^{-6}\ in^4)$
* $\underline{F = 0.985}$

3290 TYPE- Before Cracking:

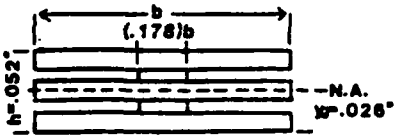

3290-type equivalent structure

$(\sigma_{max})_{al} = My/I$
$(\sigma_{max})_{pr} = nMy/I$

$n = E_{pr}/E_{al} = 1.9Msi/10.6Msi = 0.178$

$y_o = \Sigma Ay/\Sigma A = 0.026"$ (symmetry)

$I = \Sigma (bh^3/12 + Ad^2) = 5.168 \times 10^{-6}\ in^4$

* $(\sigma_{max})_{al} = My/I = (3.51\ lbs)(1.813")(\pm 0.026")/(5.168 \times 10^{-6})$
$= \underline{\pm 32.0\ ksi}$

* $(\sigma_{max})_{pr} = nMy/I = (0.178)(3.51)(1.813)(\pm 0.014)/(5.168 \times 10^{-6})$
$= \underline{\pm 3.1\ ksi}$

Correction Factor F for initial load calculation:

$F = I/I_o$
$F = (5.168 \times 10^{-6}\ in^4)/(5.859 \times 10^{-6}\ in^4)$
* $\underline{F = 0.882}$

2024-T8 Aluminum Sheet:

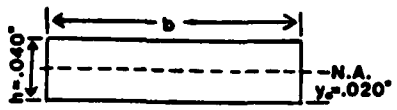

2024-T8 Aluminum

$\sigma_{max} = My/I$

$y_o = \Sigma Ay/\Sigma A = 0.020"$ (symmetry)

$I = (bh^3/12 + Ad^2) = 2.667 \times 10^{-6}\ in^4$

* $(\sigma_{max})_{al} = My/I = (2.36\ lbs)(1.813")(\pm 0.020")/(2.667 \times 10^{-6})$
$= \underline{\pm 32.0\ ksi}$

APPENDIX B

FLEXURAL STRESS ANALYSIS FOR FATIGUED ARALL

5400 TYPE- After Cracking: For the observed condition of all aluminum layers cracked except center one, remaining load of 8.34 lbs. (5405, 3 X 10^6 cycles)

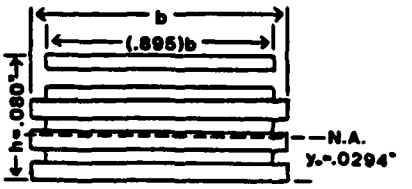

5400-type equivalent structure

$(\sigma_{max})_{al} = My/I$
$(\sigma_{max})_{pr} = nMy/I$

$n = E_{pr}/E_{al} = 9.5Msi/10.6Msi = 0.895$

$y_o = \Sigma Ay/\Sigma A = 0.0349"$ (no symmetry)

$I = \Sigma (bh^3/12 + Ad^2) = 3.088 \times 10^{-5}\ in^4$

* $(\sigma_{max})_{al} = My/I = (8.34\ lbs)(1.813")(-0.0349")/(3.088 \times 10^{-5})$
$= \underline{-34.2\ ksi}$

* $(\sigma_{max})_{pr} = nMy/I = (0.895)(8.34)(1.813)(0.0451)/(3.088 \times 10^{-5})$
$= \underline{39.5\ ksi}$

* $(\sigma_{min})_{pr} = nMy/I = (0.895)(8.34)(1.813)(-0.0229)/(3.088 \times 10^{-5})$
$= \underline{-20.1\ ksi}$

$(R_{pr} = -0.51)$

3200 TYPE- After Cracking: For the observed condition of all aluminum layers cracked except center one, remaining load of 2.45 lbs. (3204-7, 3 X 10^6 cycles)

$(\sigma_{max})_{al} = My/I$
$(\sigma_{max})_{pr} = nMy/I$

$n = E_{pr}/E_{al} = 9.5Msi/10.6Msi = 0.895$

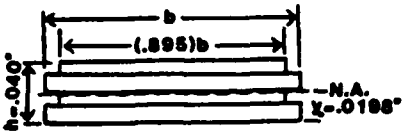

3200-type equivalent structure

$y_o = \Sigma Ay/\Sigma A = 0.0197"$ (no symmetry)

$I = \Sigma (bh^3/12 + Ad^2) = 2.547 \times 10^{-6}$ in^4

* $(\sigma_{max})_{al} = My/I = (2.45 \text{ lbs})(1.813")(-0.0197")/(2.547 \times 10^{-6})$
$= \underline{-34.4 \text{ ksi}}$

* $(\sigma_{max})_{pr} = nMy/I = (0.895)(2.45)(1.813)(0.0203)/(2.547 \times 10^{-6})$
$= \underline{31.7 \text{ ksi}}$

* $(\sigma_{min})_{pr} = nMy/I = (0.895)(2.45)(1.813)(-0.0077)/(2.547 \times 10^{-6})$
$= \underline{-12.0 \text{ ksi}}$

$(R_{pr} = -0.38)$

DISTRIBUTION LIST (Continued)
Report No. NADC-90073-60

No. of Copies

Materials Sciences Corporation 2
930 Harvest Drive, Suite 300
Blue Bell, PA 19422
(2 for Dr. S. Chatterjee)

Naval Air Development Center 12
Warminster, PA 18974-5000
(10 for Code 6063; J. Cook)
(2 for Code 8131)

Naval Aviation Depot 1
Naval Air Station
Code 340
Alameda, CA 94501-5201

Naval Aviation Depot 1
Naval Corps Air Station
Code 340
Cherry Point, NC 28533-5030

Naval Aviation Depot 1
Naval Air Station
Code 340
Jacksonville, FL 32212

Naval Aviation Depot 1
Naval Air Station
Code 340
Norfolk, VA 23511-5899

Naval Aviation Depot 1
Naval Air Station
Code 340
Pensacola, FL 32508-5300

Naval Aviation Depot 1
North Island
Code 340
San Diego, CA 92135-5112

Naval Air Systems Command 2
Washington, DC 20361-0001
(1 for AIR 5304; J. Collins)
(1 for AIR-931; L. Sloter)

Naval Air Test Center 1
Patuxent River, MD 20670-5304

DISTRIBUTION LIST (Continued)
Report No. NADC-90073-60

	No. of Copies
Naval Research Laboratory 4555 Overlook Ave. S.W. Washington, DC 20375 (1 for Code 6370) (1 for Code 6120)	2
Naval Safety Center NAS, Norfolk, VA 23511	1
Naval Sea Systems Command Washington, DC 20362	1
Naval Ship Engineering Center Washington, DC 20360 (1 for Code 6101E)	1
Naval Surface Weapons Center Silver Spring, MD 20903 (1 for D. Divecha)	1
Office of Naval Research Washington, DC 20350 (1 for Code 1131: G. Yoder)	1
Office of Naval Technology Washington, DC 20390 (2 for Code 225; J. Kelly and M. Kinna)	2
U.S. Naval Academy Department of Mechanical Engineering Annapolis, MD 21401 (2 for D. Hasson)	2
Center for Naval Analysis 4401 Fort Avenue P.O. Box 16268 Alexandria, VA 22302-0268	1

DISTRIBUTION LIST
Report No. NADC-90073-60

No. of Copies

Akzo Fibers and Polymers 2
Velperweg 76, P. O. Box 9300
6800 S.B. Arnhem
The Netherlands
(1 for Dr. M. Verbruggen)
(1 fore G.H.J.J. Roebroeks)

Alcoa Laboratories 2
Alcoa Center, PA 15069
(1 for Larry Meuller)
(1 for R. Bucci)

Alcoa 1
1615 M. Street, N.W. - Suite 500
Washington, D.C. 20036
(1 for Pamela Patrick)

Annapolis Laboratory 1
David Taylor Research Center Detachment
Annapolis, MD 21402-1198

Army Materials Technology Laboratory 1
Watertown, MA 02172-0001

Battelle Memorial Institute 1
Columbus Laboratories
505 King Ave.
Columbus, OH 43201

Center for Naval Analysis 1
4401 Fort Avenue
P.O. Box 16268
Alexandria, VA 22302-0268

Defense Technical Information Center 2
Attn: DTIC-FDAB
Cameron Station, Bldg. 5
Alexandria, VA 22314

Department of Energy 1
100 Independance Ave. S.W,
Washington, DC 20585
(1 for Code CE142)

Lehigh University 1
Coxe Laboratory
Bethlehem, PA 18015
(1 for G. Connelly)